

On the effect of a thin liquid film on the crown propagation in drop impact studies

G. Lamanna^{1*}, A. Geppert¹, B. Weigand¹

¹Institute of Aerospace Thermodynamics, University of Stuttgart, Germany

*Corresponding author: grazia.lamanna@itlr.uni-stuttgart.de

Abstract

Drop impact on a dry/wetted wall is of relevance to many industrial applications as well as to natural sciences. For some applications, such as spray coating or icing of plane wings, both the maximum spreading diameter and the residual thickness of the wall film are of paramount importance for the efficient design and optimisation of the different technologies. In this paper, we propose a modification to existing models for crown propagation and residual film thickness based on stagnation-point flow solutions. It is generally accepted that the position of the crown base exhibits a square-root dependence on time, whereby the constant of proportionality C is inversely proportional to the fourth root of the initial film thickness h_0 . We introduce the following two modifications. First, we include the thinning of the initial film thickness, which is no longer considered to be constant. The evolution of the film thickness is obtained directly from the potential flow theory for stagnation-point flow. Second, the constant C is modified to include the momentum losses in the spreading lamella due to boundary layer effects. For the estimation of viscous losses, two different exact solutions of the Navier-Stokes equations are considered with different boundary conditions. The first analytical solution is based on the classical Hiemenz flow solution for droplet impingement on a dry wall. In the second approach, the classical Hiemenz solution is extended to orthogonal stagnation-point flow against a fluid film, resting against a plane wall. This second approach enables for the first time to evaluate the effect of sliding on the crown propagation due to the presence of a liquid wall film. A comparison of the two solutions for the standard and extended Hiemenz-flow is discussed for a few representative test cases. Both solutions lead to a significant improvement in the prediction of the crown propagation rate compared to inviscid models. The preliminary results show that the inclusion of sliding effects becomes increasingly important with increasing wall films thickness ($\delta = h_0/D_0 > 0.3$), where the inception of viscous losses is temporally delayed, as confirmed by experiments. The advantages of the stagnation-point flow approach are twofold. First, it enables a smooth transition from the inertia-driven to the viscous-controlled regime of crown propagation. Second, it lays the foundation for modelling continuously the transition from low-viscosity to high-viscosity wall films and for assessing how the viscosity ratio affects the spreading rate of the crown.

Keywords

Droplet impact, sliding and viscous effects on crown propagation.

Introduction

Drop impact on a dry/wetted wall is of relevance to many industrial applications as well as to natural sciences, such as soil erosion, pesticide sprays, spray coating and IC engines. Immediately after the impact, the droplet diameter expands radially along the surface and may generate an upward growing crown, provided the impact kinetic energy is sufficiently high (splashing regime). For some specific applications, such as spray coating or icing of plane wings, both the maximum spreading diameter and the residual thickness of the wall film are of paramount importance for the efficient design and optimisation of the different technologies. From a theoretical point of view, it is generally agreed to model the crown as a kinematic discontinuity, thereby neglecting the influence of viscous losses. This assumption dates back to the pioneering work of Yarin and Weiss [1], who proposed a theoretical square-root dependence for the crown base radius R_{Base} upon the non-dimensional time τ : $R_{Base} = C\sqrt{(\tau - \tau_0)}$. Here τ_0 corresponds to the initial value at the moment of impact. The non-dimensional constant C was determined empirically by fitting the experiments of Levin and Hobbs [2], according to $C = [2/(3\delta)]^{1/4}$. The square-root dependence is adopted by several authors with slight modifications to the empirical constant C [3, 4, 5, 6]. A controversial issue is whether the parameter C depends also on the Weber and Reynolds number. According to Refs. [6, 3, 7, 8], the crown diameter is independent of the Weber and Reynolds number. This conclusion, however, is not shared by Fujimoto et al. [9], who showed that surface tension plays an important role on the evolution of the crown diameter. This controversy was recently clarified by Gao and Li [10], who introduced a correction factor λ_0 to the parameter $C = [2\lambda_0^2/(3\delta)]^{1/4}$ to take into account the liquid film inertia and the energetic losses due to deformation. This basically implies the velocity of crown propagation in the inviscid theory is reduced compared to the impact velocity by the factor λ_0 ($u_\infty = \lambda_0 U_0$). The latter was determined empirically according to $\lambda_0 = 0.26Re^{0.05}/(We^{0.07}\delta^{0.34})$. The correlation shows that the dominating effect is provided by liquid inertia and only a weak dependence on We and Re is observed. These findings have been confirmed by the numerical simulations of Davidson [11], who showed that, at the moment of impact, surface energy losses can amount up to 10% of the total impact kinetic energy. Geppert et al. [12] compared the predictions from different models with experiments. The results are summarised in Figure 1 for two representative models and two different non-dimensional wall film thicknesses. As can be seen, all inviscid models overestimate the spreading rate of the crown base radius and exhibit a reverse δ -dependency with

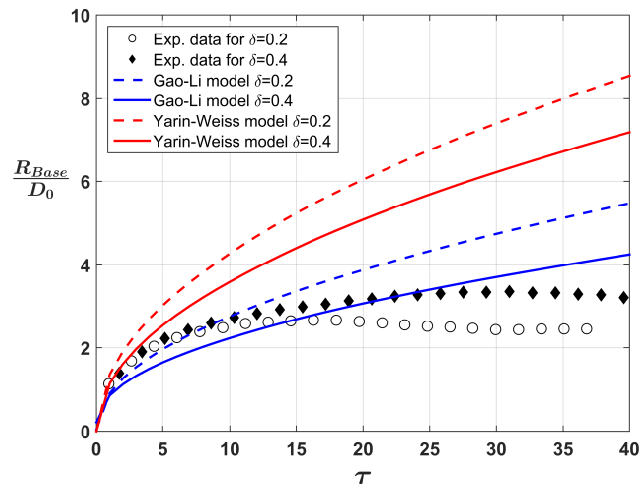


Figure 1. Temporal evolution of the crown base radius: comparison between experiments and inviscid models. Fluids: *n*-hexadecane for both droplet and wall film. $We \approx 1330$.

respect to the experiments. For inviscid theories, with increasing δ the wall film inertia increases, thus resulting in a slower spreading rate. In the experiments, the opposite is observed. Three elements can contribute to explain this discrepancy: the sliding of the impacting droplet on the wetted wall and boundary layer effects, enhanced by the decrease of the wall film height during the spreading of the crown. Sliding effects have never been investigated either experimentally or theoretically. Boundary layer effects have been studied by several authors [5, 13, 14]. Marcotte et al. [14] showed that the crown spreading consists out of two distinct sheets, originating from the droplet and liquid film, respectively. They evolve on separate timescales and the merging time is mainly depending upon the viscosity ratio. Roisman [13] solved analytically the axisymmetric stationary viscous flow in a spreading film, generated by normal drop impact onto a rigid, planar, dry substrate. He also provided an expression for calculating the height of the residual film thickness. The existence of a residual film thickness has been confirmed experimentally also by Kuhlman et al. [15]. The authors measured the cavity film thickness for single droplet impact on a wetted wall in the range $140 \leq We \leq 1000$ and $0.2 \leq \delta \leq 1.0$ and demonstrated the existence of a constant thickness region (sub-cavity) within the crown base area. Despite the noteworthy progress, none of the above studies led to the formulation of a model for the crown spreading rate that encompasses all the above mentioned effects.

In this paper, we present an analytical approach based on stagnation-point flow. It includes two different exact solutions of the Navier-Stokes equations, obtained for different boundary conditions. The first analytical solution is based on the classical Hiemenz flow solution for droplet impingement on a dry wall. A detailed description of this method can be found in [16]. In the second approach, the classical Hiemenz solution is extended to orthogonal stagnation-point flow against a fluid film, resting on a plane wall. This second approach enables for the first time to evaluate the effect of sliding on the crown propagation due to the presence of a liquid wall film.

Analytical solutions for stagnation-point flow

The modelling strategy is based on the geometrical resemblance of the droplet impact against a solid substrate and the two-dimensional, orthogonal stagnation-point flow (SPF), as shown in Figure 2 for impact on a dry surface and on a liquid film. From a mathematical point of view, the main difference between the two configurations is the inclusion of a free surface, where a kinematic condition of equal velocities and tangential stresses is applied between the upper and lower fluid. The origin of the coordinate system is set at the point P (stagnation point) with the coordinate axis directed as shown in Figure 2(a). In both configurations, the impacting droplet transmits a contact impulse to the liquid substrate, which is pushed down towards the wall. In our approach, the decay of the wall-film height is derived directly from the potential theory for stagnation-point flow. The momentum losses, associated with the spreading of the liquid film parallel to the wall, are estimated by employing the similarity solution for the velocity components in the ensuing boundary layer (Hiemenz flow) [19].

Decay rate of the film thickness

We assume that far away from the solid wall, the flow distribution within the impacting droplet is a frictionless potential flow (see Figure 2). The x - and y -velocity components of the potential flow can be expressed as $u = ax$ and $v = -ay$, where a is the strength of the potential flow. Its value can be estimated either through a semi-empirical procedure described in [16], or from the initial conditions $a = \lambda_0 U_0 / D_0$. Basically, the constant a represents the momentum per unit length transmitted by the droplet to the liquid film at the moment of impact. Indicating with h_0 the initial wall film thickness, the decrease in wall film thickness can be expressed as $h(t) = h_0 - ayt$. Being at each time instant $h(t) = y$, it yields [18]

$$h(t) = \frac{h_0}{1 + at}. \quad (1)$$

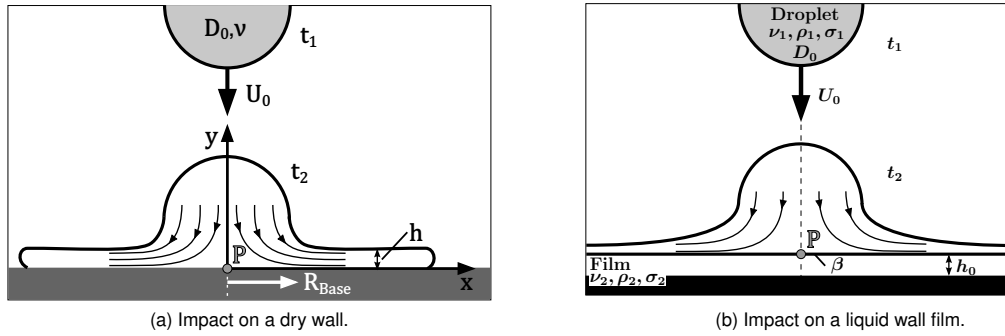


Figure 2. Schematic drawing of the droplet impact against a dry wall (a) and a liquid wall film (b), respectively.

Equation 1 implicitly assumes that there are no losses in the transmission of momentum from fluid 1 to fluid 2. This assumption is fulfilled for low viscosity fluids, such as *n*-hexadecane considered in this work for both the upper and lower fluid. For fluids with higher viscosity, momentum losses may need to be included in the estimation of the factor a . Figure 3 shows the decay of the wall film thickness for three representative test cases, discussed in Figure 9. The horizontal lines represent the thickness of the flow boundary layer $h_{BL} = 2.4\sqrt{\nu/a}$. As can be seen, the assumption of inviscid flow is justified only in the initial phase of crown propagation until the intersection with the boundary layer height h_{BL} . This explains why, for the ($\delta = 0.2$) case in Figure 1, the Gao and Li [10] model starts deviating from the experiments as of $\tau \approx 5$, which corresponds to a physical time $t \approx 2.5$ s in Figure 3. Note that the importance of boundary layer effects increases with decreasing initial film height h_0 . As a result, the discrepancy between inviscid models and experiments increases accordingly.

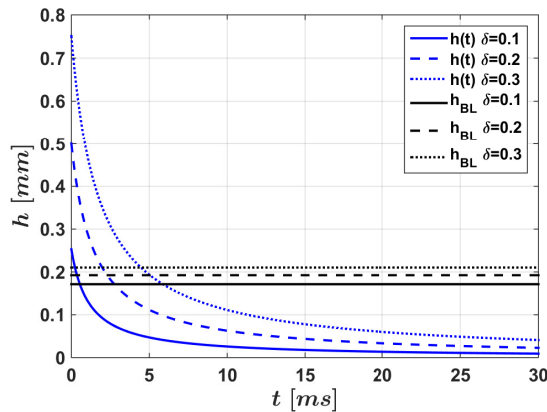


Figure 3. Temporal evolution of the wall film height for the experiments shown in Figure 9, where test conditions and a values are specified. In the figure h_{BL} denotes the thickness of the boundary layer.

Extended Hiemenz flow

Following the methodology laid out by Hiemenz for impact on a dry wall, as described in Schlichting and Gersten [19], and by Wang [17] for impact on a liquid film, one seeks a similarity solution for the velocity components in both fluid layers (1 and 2). The coordinate system in the self-similar domain is shown in Figure 6 for both configurations. For the upper fluid (1), it holds

$$\eta = \sqrt{\frac{a}{\nu_1}} y, \quad f(\eta) = \frac{\psi}{x\sqrt{\nu_1 a}}, \quad u_1 = axf'(\eta) \quad v_1 = -\sqrt{\nu_1 a} f(\eta) \quad (2)$$

where ψ is the stream function and u_1, v_1 are the velocity components in the upper fluid of the stagnation-point flow. The transformed ordinary differential equation reads then as follows:

$$f'''(\eta) + ff'' - f'^2 + 1 = 0 \quad (3)$$

subject to the boundary conditions of sliding (β) at the interface ($\eta = 0$) and inviscid flow limit ($\eta \rightarrow \infty$):

$$\eta = 0: \quad f = 0, \quad f' = \beta; \quad \eta \rightarrow \infty: \quad f' = 1. \quad (4)$$

Hence, the variable β represents the non-dimensional tangential component of the fluid velocity at the interface. Its value varies from zero (solid boundary) to one (inviscid boundary). Hence, for $\beta = 0$ we recover the classical

Hiemenz solution and for $\beta = 1$ the solution for fluid 1 is potential ($f = \eta$). Three representative self-similar profiles for the function f and its first derivative are shown in Figure 4. For the lower fluid (2), it holds

$$\zeta = \sqrt{\frac{a}{\nu_2 \beta}} y_2, \quad u_2 = a\beta x g'(\zeta), \quad v_2 = -\sqrt{\nu_2 a \beta} g(\zeta) \quad (5)$$

and the Navier-Stokes equations reduce to

$$g'''(\zeta) + g g'' - g'^2 = 0 \quad (6)$$

with no-slip boundary conditions at the solid wall ($\zeta \rightarrow \infty$) and equal tangential velocities ($u_1 = u_2$) at the interface ($\zeta = 0$):

$$\zeta = 0: \quad g = 0, \quad g' = 1; \quad \zeta \rightarrow \infty: \quad g' = 0. \quad (7)$$

Contrary to the function $f(\eta)$, the function $g(\zeta)$ is universal and independent of β . For the two-dimensional SPF, it is possible to find a closed form solution for equation (6) [17]:

$$g = 1 - e^{-\zeta}. \quad (8)$$

The variation of the function g and its derivative g' in the self-similar domain is depicted in Figure 5 (a).

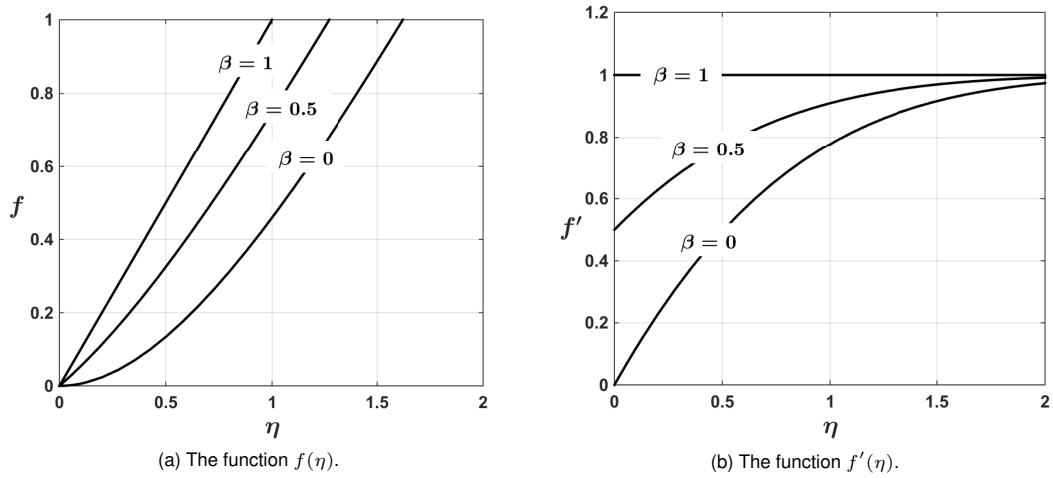


Figure 4. Extended Hiemenz similarity solution for different values of the constant β in the upper fluid layer.

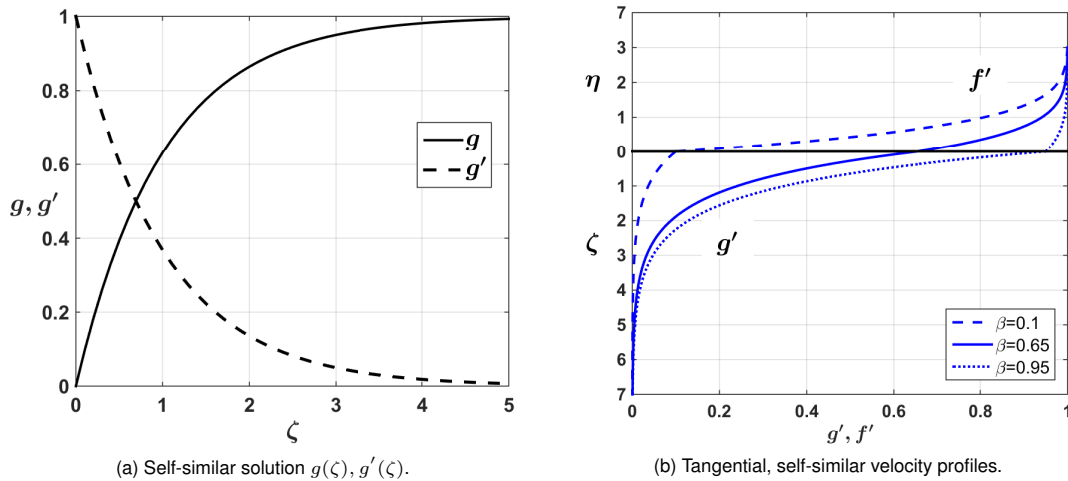


Figure 5. (a) Self-similar solution in the lower fluid layer. (b) Coupling of the self-similar solutions for different sliding values (β).

The final step is then to determine the appropriate sliding value β for a given droplet impact experiment. Following Wang [17], the factor β can be derived by imposing continuity of tangential stresses at the interface:

$$\rho_1 \nu_1 \frac{\partial u_1}{\partial y} = -\rho_2 \nu_2 \frac{\partial u_2}{\partial y}. \quad (9)$$

This yields the following relation for determining β through an iterative procedure:

$$\frac{f''(0)}{-\beta^{3/2} g''(0)} = \frac{\rho_2}{\rho_1} \left(\frac{\nu_2}{\nu_1} \right)^{1/2} = K. \quad (10)$$

The results of this exercise are presented in [17] and have been summarised here in the following correlation

$$\beta = 0.548 e^{-0.7456K} + 0.4195 e^{-0.05873K}. \quad (11)$$

As soon as the factor β is known, the self-similar solution for the upper fluid can be determined numerically with a shooting method. The coupling of the solutions for three representative cases is illustrated in Figure 5 (b). Note that, due to the kinematic condition ($u_1 = u_2$), the curve $g'(\zeta)$ is scaled with β and vanishes for $\beta = 0$. The opposite is observed for $\beta = 1$, where no losses are predicted and the interface velocity converges towards the inviscid limit: $f' = g' = 1$ and hence $u_1 = u_2 = ax$.

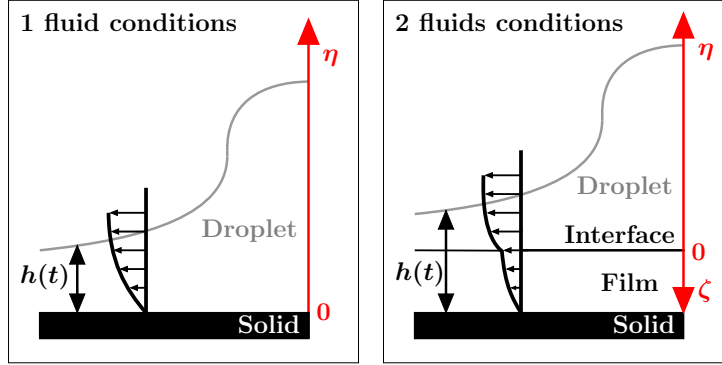


Figure 6. Schematic drawing of the velocity profile in the boundary layer for the one and two-fluids configurations, together with the associated self-similar coordinate systems.

Results and discussion

This section describes our method for estimating the momentum losses and its integration in current inviscid models for crown propagation. This approach enables a continuous, smooth transition from the inertia-driven (negligible losses) to the viscous-controlled regime of crown propagation.

Estimation of momentum losses

The self-similarity of the solution of the extended Hiemenz flow allows for a straightforward estimation of momentum losses in the boundary layer. The latter can be estimated by introducing a profile-averaged non-dimensional velocity in both the upper and lower fluid according to:

$$\frac{\bar{u}}{u_\infty} = \frac{1}{\zeta_{max}} \int_{\zeta_{max}}^0 \beta g' d\zeta + \frac{1}{\eta_{max}} \int_0^{\eta_{max}} f' d\eta \quad (12)$$

where ζ_{max} represents the total height of the lower fluid in self-similar coordinate. For all practical purposes, it can be assumed ($\zeta_{max} = 7$), being $g'(7) = 0$. As pointed out in [20], the solution $g(\zeta)$ is equivalent to that of a stretching plate, where the vorticity created at the plate is confined to a region near the wall of thickness ζ_{max} . In the droplet impact problem, the stretching plate is replaced by the interface between the two liquids, as shown in Figure 6. The height of the upper fluid layer η_{max} converges to the potential flow solution and hence coincides with the scaled height of the wall film in the physical coordinate system, i.e. $\eta_{max} \sqrt{a/\nu_1} h(t)$. At the instant of impact, due to sliding effects, part of the fluid in the lower layer is pushed outwards so that the interface between the two fluids is located below h_0 . Its position in the physical coordinate system is not known. However, in the self-similar domain, it is always conveniently located at ($\eta = \zeta = 0$), so that equation (12) can be integrated directly without requiring the accurate tracking of the interface location in time. Finally, the classical Hiemenz solution is recovered automatically, being $g'(\zeta) = 0, \forall \zeta$. This implies that the presence of the wall is felt immediately across the entire film height. The integration of equation (12) yields:

$$\frac{\bar{u}}{u_\infty} = \beta \frac{g(0)}{\zeta_{max}} + \frac{f(\eta_{max})}{\eta_{max}} \quad (13)$$

It is important to realise that not only η_{max} , but also β is not constant in time. Specifically, we made the following assumptions:

1. If $h(t) > h_{BL}$, it holds $\beta = K = \frac{\rho_2}{\rho_1} \left(\frac{\nu_2}{\nu_1} \right)^{1/2}$.
2. If $h(t) < h_{BL}$, the tangential velocity (sliding) at the interface starts to decrease, yielding $\beta(t) = \beta(t-1)g'(\zeta)$. In other words, the self-similar solution $g(\zeta)$, which is independent of β , provides the rate of decrease of the tangential velocity/sliding with decreasing film height.

As an example, the temporal evolution of the parameter β is shown in Figure 7 (a) for two different film heights. All experimental conditions are provided in Figure 9. As can be seen, the lower the non-dimensional film height, the earlier the parameter β approaches the dry-wall solutions ($\beta = 0$). With increasing film height, the sliding remains constant over a longer time, thus inducing minor momentum losses in the upper layer, as shown in Figure 7 (b). Consequently, the discrepancy in predicted momentum losses between the 1-fluid and 2-fluid approach increases with increasing film height (see Figure 7 (b)). Note that the most significant part of the momentum losses occurs in the upper fluid, as shown in Figure 8 for a representative test case. As mentioned earlier, the lower fluid can be mainly considered as a vorticity layer, which is then convected away as soon as its thickness vanishes. Despite this uneven repartition, it is clear that the total momentum losses due to viscous effects cannot be neglected during a significant portion of the crown propagation, particularly for thin wall films. This explains the discrepancy between inviscid models and experiments, observed in Figure 1. Note that η_{max} decays in time with the film thickness, being $\sqrt{a/\nu} h(t)$. Hence the profile-averaged velocity is calculated over an increasingly smaller length scale, thus inducing a significant increase in momentum losses.

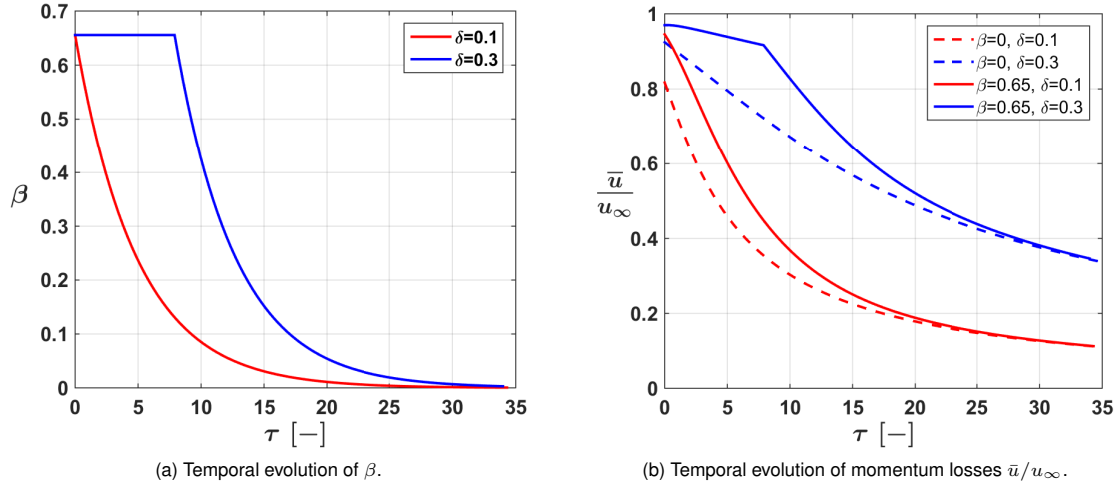


Figure 7. Temporal evolution of the sliding parameter β (a) and of the total momentum losses \bar{u}/u_∞ (b) for two representative experiments. The corresponding test conditions are specified in Figure 9.

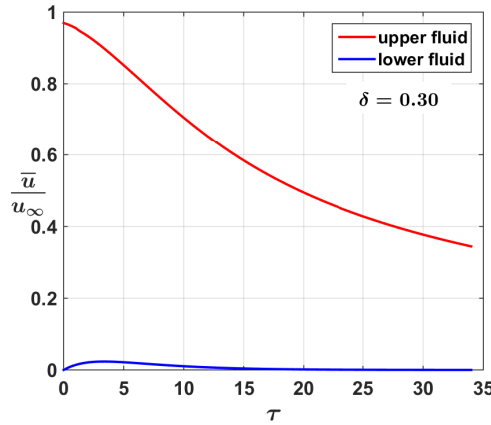


Figure 8. Temporal evolution and repartition of momentum losses between the upper and lower fluid layer. Fluids: *n*-hexadecane for both droplet and wall film. $We \approx 1330$

The above estimation of momentum losses can now be incorporated in the modelling of the crown propagation. As a first step, the averaged velocity is transformed back to the physical coordinate system according to

$$\frac{\bar{u}}{u_\infty} = \beta(t) \frac{1}{7\sqrt{\nu_2\beta/a}} + \frac{1}{\sqrt{\frac{a}{\nu}}h(t)} f\left(\sqrt{\frac{a}{\nu}}h(t)\right). \quad (14)$$

Recall that u_∞ denotes the velocity outside the boundary layer as determined by potential theory and set equal to $u_\infty = \lambda_0 U_0$. As stated earlier, this choice takes into account the energetic losses due to deformation during droplet impact. Following Gao and Li [10], we can define a new correction factor λ_{AG} according to

$$\lambda_{AG} = \frac{\bar{u}}{U_0} = \lambda_0 \left[\beta(t) \frac{1}{7\sqrt{\nu_2\beta/a}} + \frac{1}{\sqrt{\frac{a}{\nu}}h(t)} f\left(\sqrt{\frac{a}{\nu}}h(t)\right) \right]. \quad (15)$$

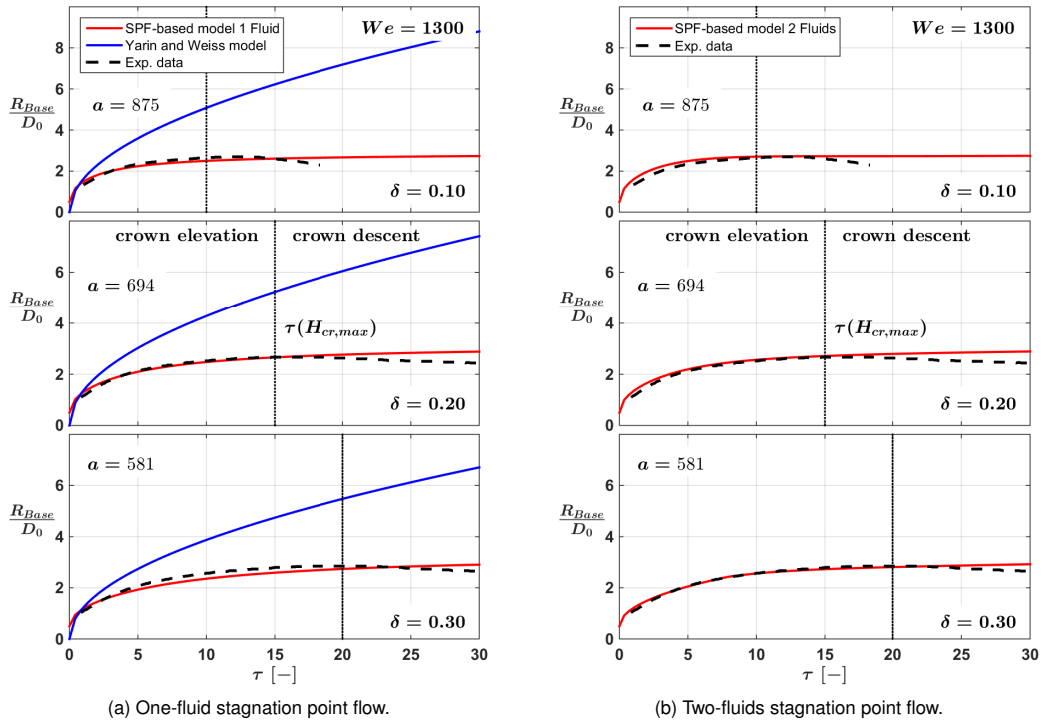


Figure 9. Temporal evolution of the crown base radius: comparison between experiments, an inviscid model [1] and SPF-based models. Fluids: n -hexadecane for both droplet and wall film. $We \approx 1330$.

Finally, the crown base propagation is modelled as follows

$$\frac{R_{Base}}{D_0} = 0.5 + \left(\frac{2\lambda_{AG}^2}{3\delta} \right)^{1/4} \sqrt{\tau}. \quad (16)$$

The use of the variable factor λ_{AG} takes into account the effect of increasing viscous losses during crown propagation. The initial value τ_0 can be set to zero, because the time origin is known accurately. The tracking of the crown radius starts as soon as the droplet is no longer visible in the images. This occurs approximately when the crown radius equals the droplet radius, thus explaining the 0.5 shift. The classical Hiemenz solution is recovered immediately by setting the value of β to zero in Eq. (15). A comparison between the 1-fluid and 2-fluids solutions is shown in Figure 9 for three representative experiments. As can be seen, for $\delta < 0.3$, both solutions provide almost identical results. Due to the rapid decay of the sliding parameter, the 2-fluids solutions rapidly draw near to the classical Hiemenz solutions and only minor deviations are obtained in the associated $f(\eta)$ profiles. For the $\delta = 0.3$, the presence of significant sliding effects over a prolonged time reduces the momentum losses. This effect can only be reproduced by the 2-fluids approach, leading to a more accurate prediction of the crown spreading rate.

The proposed modelling strategy provides a significant step forward in the prediction and understanding of crown propagation on wetted walls. It also provides a logical explanation for the reverse δ -dependence observed in the experiments with respect to inviscid models. In addition, based on the recent findings from Marcotte et al. [14], it provides a straightforward explanation for the different timescales observed numerically on the spreading rate of the corolla.

Conclusions

This paper discusses a new approach for modelling the crown propagation, based on stagnation-point flow solutions. We mainly introduce the following two modifications. First, the initial film thickness is no longer considered a constant. The evolution of the film thickness is obtained directly from the potential flow theory for stagnation-point flow. Second, we include an estimation of momentum losses in the modelling of the lamella's spreading rate due to boundary layer effects. For the estimation of viscous losses, two exact solutions of the Navier-Stokes equations are considered with different boundary conditions: impact on a dry wall (Hiemenz flow) and on a liquid film, resting against a plane wall (extended Hiemenz flow). This second approach allows, for the first time, to evaluate the effect of sliding on the crown propagation due to the presence of a liquid wall film. The shear stresses at the interface between the two fluids create a vorticity layer, close to the wall, that acts as buffer and reduces the momentum losses in the upper fluid layer. As a result, momentum losses are significantly reduced with increasing initial film thickness. This trend is corroborated by experiments, while inviscid models lead to opposite conclusions. For thin liquid films ($\delta \leq 0.2$), the sliding parameter β decreases very rapidly and the prediction of momentum losses in the 1-fluid and 2-fluids solutions are basically identical. The latter are estimated by introducing profile-averaged velocities for both fluid layers. Our analysis shows that the momentum losses are negligible in the early phase of crown propagation and become increasingly important with reducing film height. This enables a smooth transition

from the inertia-driven to the viscous-controlled regime of crown propagation.

More in general, the present work lays the foundation for analysing the effect of sliding for droplet impingement on wall films of different viscosity. This will enable, for the first time, to model continuously the transition from low-viscosity to high-viscosity wall films and assess how the viscosity ratio affects the overall crown spreading and splashing dynamics.

Acknowledgements

The authors wish to thank the Deutsche Forschungsgemeinschaft (DFG) for financial support in the framework of the projects LA 2512/2-1, WE 2549/24-1 and GRK 2160/1 “Droplet Interaction Technologies” (DROFIT).

Nomenclature

a	strength of the potential flow [s^{-1}], $a = U_0/D_0$
β	self-similar tangential velocity component at the interface [-]
C	proportionality constant [-], $C = 2\lambda_{AG}^2/(3\delta)$
δ	non-dimensional film thickness [-], $\delta = h_0/D_0$
D_0	initial droplet diameter [m]
η	self-similar coordinate normal to the solid wall for fluid 1 [-], $\eta = y\sqrt{a/\nu_1}$
F	force [N]
h_0	initial wall film height [m]
K	non-dimensional flow constant [-], $K = \rho_2/\rho_1(\nu_2/\nu_1)^{(1/2)}$
λ_0	correction factor encompassing deformation losses [-]
λ_{AG}	new correction factor encompassing deformation and viscous losses [-]
ν	kinematic viscosity [m^2/s]
R_{Base}	crown base radius [m]
Re	Reynolds number [-], $\rho U_0 D_0/\mu$
ρ	density [kg/m ³]
σ	surface tension [N/m]
τ	non-dimensional time [-], $\tau = tU_0/D_0$
t	time [s]
U_0	droplet impact velocity [m/s]
We	Weber number [-], $\rho U_0^2 D_0/\sigma$
x	coordinate for the horizontal axis [m]
y	coordinate for the vertical axis [m]
y_2	coordinate for a second vertical axis for fluid 2 [m]
ζ	self-similar coordinate normal to the solid wall for fluid 2 [-], $\zeta = y_2\sqrt{a/(\nu_2\beta)}$
SPF	Stagnation Point Flow

References

- [1] Yarin, A. L., and Weiss, D. A., 1995, *Journal of Fluid Mechanics*, 283, pp.1-33.
- [2] Levin, Z., and Hobbs, P. V., 1971, *Royal Society Publishing*, 269, pp. 555-585.
- [3] Rieber, M., and Frohn, A., 1999, *International Journal of Heat and Fluid Flow*, 20, 455-461.
- [4] Cossali, G. E., Marengo, M., Coghe, A., and Zhdanov, S., 2004, *Experiment in Fluids*, 36(6), pp. 888-900.
- [5] Trujillo, M. F., and Lee, C. F., 2001, *Physics of Fluids*, 13(9), 2503.
- [6] Liang, G., Guo, Y., Shen, S., and Yang, Y., 2014, *Theoretical and Computational Fluid Dynamics*, 28(2), pp. 159-170.
- [7] Josserand, C., and Zaleski, S., 2003, *Physics of Fluids*, 15, pp. 1650-1657.
- [8] Agbaglah, G., and Deegan, R. D., 2014, *Journal of Fluid Mechanics*, 752, pp. 485-496.
- [9] Fujimoto, H., Ogino, T., Takuda, H., and Hatta, N., 2001, *International Journal of Multiphase Flow*, 27 pp. 1227-1245.
- [10] Gao, X., and Li, R., 2015, *Physical Review E*, 92, pp. 053005.
- [11] Davidson, M. R., 2002, *Chemical Engineering Science*, 57, pp. 3639-3647.
- [12] Geppert, A., Terzis, A., Lamanna, G., Marengo, M., and Weigand, B., 2017, *Experiment in Fluids*, 58, pp. 172.
- [13] Roisman, I. V., 2009, *Physics of Fluids*, 21, pp. 052104.
- [14] Marcotte, F., Michon, G.-J., Séon, T., and Josserand, C., 2019, *Physics Review Letters*, 122, pp. 014501
- [15] Kuhlman, J. M., and Hillen, N. L., 2016, *Experimental Thermal and Fluid Science*, 77, pp. 246-256.
- [16] Lamanna, G., Geppert, A., and Weigand, B., 2017, *Physics Review Letters*, (submitted).
- [17] Wang, C. Y., 1985, *Quarterly of Applied Mathematics*, 43(2), pp. 215-223.
- [18] Blyth, M., and Pozrikidis, C., 2005, *Acta Mechanica*, 180, pp. 203-219.
- [19] Schlichting, H., and Gersten, K., 2017, “Boundary-Layer Theory”. Springer-Verlag Berlin Heidelberg, 9th edition.
- [20] Drazin, P., and Riley, N., 2007, “The Navier-Stokes Equations: A Classification of Flows and Exact Solution”. Lecture Note Series 334, Cambridge University Press, 2nd edition.